0013-7227/04/$15.00/0
Printed in U.S.A.

Endocrinology 145(11):5269–5279

doi: 10.1210/en.2004-0233

Transgenic Mice Overexpressing Human Fibroblast Growth Factor 23 (R176Q) Delineate a Putative Role for Parathyroid Hormone in Renal Phosphate Wasting Disorders

XIUYING BAI, DENGSHUN MIAO, JIARONG LI, DAVID GOLTZMAN, AND ANDREW C. KARAPLIS

Division of Endocrinology (X.B., A.C.K.), Department of Medicine, and Lady Davis Institute for Medical Research, Sir Mortimer B. Davis-Jewish General Hospital, McGill University, Montréal, Québec, Canada H3T 1E2; Calcium Research Laboratory (D.M., J.L., D.G.), Department of Medicine, McGill University Health Center and McGill University, Montréal, Québec, Canada H3A 1A1

Fibroblast growth factor 23 (FGF23) is a recently characterized protein likely involved in the regulation of serum phosphate homeostasis. Increased circulating levels of FGF23 have been reported in patients with renal phosphate-wasting disorders, but it is unclear whether FGF23 is the direct mediator responsible for the decreased phosphate transport at the proximal renal tubules and the altered vitamin D metabolism associated with these states. To examine this question, we generated transgenic mice expressing and secreting from the liver human FGF23 (R176Q), a mutant form that fails to be degraded by furin proteases. At 1 and 2 months of age, mice carrying the transgene recapitulated the biochemical (decreased urinary phosphate reabsorption, hypophosphatemia, low serum 1,25-dihydroxyvitamin D_3) and skeletal (rickets and osteomalacia) alterations associated with these disorders. Unexpectantly, marked changes in parameters of calcium homeostasis were also observed, consistent with secondary hyperparathyroidism. Moreover, in the kidney the anticipated alterations in the expression of hydroxylases associated with vitamin D metabolism were not observed despite the profound hypophosphatemia and increased circulating levels of PTH, both major physiological stimuli for 1,25-dihydroxyvitamin D_3 production. Our findings strongly support the novel concept that high circulating levels of FGF23 are associated with profound disturbances in the regulation of phosphate and vitamin D metabolism as well as calcium homeostasis and that elevated PTH levels likely also contribute to the renal phosphate wasting associated with these disorders. (*Endocrinology* 145: 5269–5279, 2004)

RENAL PHOSPHATE-WASTING disorders encompass the heritable disorders of X-linked and autosomal dominant hypophosphatemic rickets (XLH and ADHR, respectively) as well as the acquired condition of tumor-induced osteomalacia (TIO) (1–3). This group of diseases is characterized by renal phosphate excretion leading to hypophosphatemia, defective skeletal mineralization, and the clinical findings of osteomalacia and rachitic deformities of the growth plates in growing children. Accompanying these findings is a peculiar defect in vitamin D metabolism epitomized by serum levels of 1,25-dihydroxyvitamin D_3 [$1,25(OH)_2D_3$] that are inappropriately low for the degree of prevailing hypophosphatemia, a major physiological stimulus for $1,25(OH)_2D_3$ production. Hypophosphatemic rickets/osteomalacia is also recognized as a rare complication of fibrous dysplasia in either isolation or association with McCune-Albright syndrome (4).

A central role for fibroblast growth factor 23 (FGF23) in the pathogenesis of these hypophosphatemic disorders has been proposed (5–8), although other factors such as matrix extracellular phosphoglycoprotein (9) and secreted frizzled-related protein 4 (10) have also been implicated. Targeted disruption of *Fgf23* leads to high serum phosphate, increased renal phosphate reabsorption and elevation in serum $1,25(OH)_2D_3$ (11). Alternatively, increased circulating levels of FGF23 may lead to urinary phosphate wasting and altered vitamin D metabolism. Hence, impaired FGF23 degradation due to reduction or loss of phosphate-regulating gene with homologies to endopeptidases on the X chromosome (PHEX) protease activity has been suggested to underlie the XLH phenotype (12). Specific mutations of arginine residues at position 176 or 179 of FGF23 that disrupt the sequence motif recognized by furin proteases, cause ADHR presumably due to altered processing or decreased degradation of the protein (13, 14). Overproduction of FGF23 by tumors (14, 15) and osteogenic cells in fibrous dysplastic lesions (16) is likely responsible for the hypophosphatemia in TIO and fibrous dysplasia, respectively.

By implanting nude mice with tumors that oversecrete

Abbreviations: ADHR, Autosomal dominant hypophosphatemic rickets; ALP, alkaline phosphatase; APOE3, apolipoprotein E3; BMD, bone mineral density; BV, bone volume; Cyp24, 25-hydroxyvitamin D_3 24-hydroxylase; Cyp27b1, renal 25-hydroxyvitamin D_3-1α-hydroxylase; 3D, three-dimensional; FGF23, fibroblast growth factor 23; Gapdh, glyceraldehyde-3-phosphate dehydrogenase; microCT, microcomputed tomography; Npt2, sodium-phosphate transport protein 2; $1,25(OH)_2D_3$, 1,25-dihydroxyvitamin D_3; PHEX, phosphate-regulating gene with homologies to endopeptidases on the X chromosome; SDS, sodium dodecyl sulfate; SSC, saline sodium citrate; TIO, tumor-induced osteomalacia; TRAP, tartrate resistant acid phosphatase; XLH, X-linked hypophosphatemic rickets.

***Endocrinology* is published monthly by The Endocrine Society (http://www.endo-society.org), the foremost professional society serving the endocrine community.**

FGF23 into the circulation, others and we (5, 17) have shown that this model recapitulates the biochemical and histological alterations in bone associated with TIO. In addition, overexpression of the mutant FGF23 form identified in patients with ADHR FGF23 (R176Q) exerted derangements more profound than the wild-type protein, perhaps due to its prolonged biological half-life (17).

Despite significant advances in our understanding of these disorders, a number of important questions remain unanswered (18). For example, it is unclear whether circulating FGF23 levels are increased in XLH patients (14, 19–21), whether FGF23 is a direct PHEX substrate (22–24), and whether FGF23 is the direct mediator responsible for decreased transport phosphate by the proximal renal tubules and derangement in the regulation of vitamin D metabolism or whether another factor contributes to these effects (6, 18). To answer such questions, an animal model of FGF23 overexpression devoid of the potential biological pitfalls and short life span associated with tumor implantation would be desirable. Here we describe the generation of a murine model of FGF23 overexpression using a transgene encoding the secreted form of human *FGF23* (R176Q) cDNA and the evolution of associated biochemical and bone histological changes at 1 and 2 months postnatally. We report that, contrary to previous reports, increased circulating levels of FGF23 alter parameters of phosphate and vitamin D as well as calcium homeostasis and that elevated PTH levels likely contribute to the renal phosphate wasting associated with these disease states.

Materials and Methods

Transgene construct

The transgene was constructed in the pLiv plasmid (a gift from R. A. Davis, Department of Biology, College of Sciences, San Diego State University, San Diego, CA), containing the 5′ flanking sequence (3 kb), exon 1 and part of exon 2 (0.9 kb), part of 3′ flanking sequence (254 bp, including polyadenylation signal sequence), and the hepatic control region of the human *apolipoprotein E3* (*APOE3*) gene. The human *FGF23* (R176Q) cDNA, encoding the whole coding region was tagged with a *myc* (~798 bp) epitope and ligated into the pLiv plasmid at the *Mfe*I site. When expressed in cultured human hepatoma (HepG2) cells, this vector produced a band corresponding to an approximately 30-kDa protein on Western blot analysis using an anti-myc antibody (data not shown).

Generation of transgenic mice

All animal experiments were reviewed and approved by the institutional animal care committee. Transgenic mice designed to express human FGF23 (R179Q) in a liver-specific manner were generated using standard protocols. After establishing the correct orientation of the cDNA, the entire transgene was isolated from plasmid sequences by *Sac*II/*Spe*I restriction endonuclease digestion. The linearized 6.6-kb fragment was gel purified using NucleoTrap nucleic acid purification kit (Clontech, Palo Alto, CA), microinjected into single-cell C57B/6J × CBA embryos, and implanted into pseudopregnant female mice.

Identification of transgenic mice and establishing transgenic lines

Mice were screened for integration of the transgene by Southern blot analysis of tail DNA. Offspring from pseudopregnant foster mothers were weaned at 3 wk of age, and DNA was prepared from a 1-cm portion of their tails. In brief, 10 μg of genomic DNA were digested with *Eco*RI, separated by agarose gel electrophoresis, transferred to a nitrocellulose membrane, and hybridized with a 753-bp [α-^{32}P]dCTP-labeled h*FGF23* cDNA as probe. Signals were detected by autoradiography. Mice carrying the transgene were mated with C57BL/6J mice to generate transgenic F1 progeny.

The mice were housed in a 12-h light, 12-h dark cycle maintained in cages with wooden shavings and had free access to water and normal calcium diet (0.95% calcium, 0.67% phosphorus, 4.5 IU/g vitamin D_3; 0.21% Mg, 23.4% protein, 4.5% fat, 5.3% fiber, 6.9% ash; PMI Feeds, Inc., St. Louis, MO) in pelleted form. Weight of mice was measured every month.

Immunoprecipitation and Western blot analysis

Liver tissue (50 mg) from wild-type or transgenic mice was homogenized in 0.5 ml of radioimmunoprecipitation assay buffer [150 mM NaCl, 1% Nonidet P-40, 0.5% deoxycorticosterone, 0.1% sodium dodecyl sulfate (SDS), 50 mM Tris (pH 7.5)] supplied with a cocktail of protease inhibitors (Roche Diagnostics, Laval, Québec, Canada) and 1 mM phenylmethylsulfonyl fluoride. Extracts were clarified by centrifugation at 10,000 × *g* for 20 min at 4 C and 10 mg of liver tissue lysate were precleared by incubating with 50 μl protein G beads (Roche Diagnostics). The supernatants were then incubated with 2 μg anti-FGF23 antibody (Immutopics, Inc., San Clemente, CA) and 50 μl protein G beads with rotation overnight at 4 C, the beads were collected by centrifugation, washed twice in radioimmunoprecipitation assay buffer, dissolved in Laemmli buffer, and analyzed by SDS-PAGE (12%). The proteins were transferred to supported nitrocellulose membrane by electroblotting, followed by incubation with anti-myc monoclonal antibody (Roche Diagnostics). After the addition of a secondary horseradish peroxidase-conjugated goat antimouse IgG (Sigma, Oakville, Ontario, Canada), the membrane was subjected to enhanced chemiluminescence analysis.

Serum and urine biochemistry

Serum and urine concentrations of calcium, phosphorus, and creatinine and serum alkaline phosphatase activity were determined by routine methods using diagnostics reagents (Sigma). Tubular maximum reabsorption of phosphate per 100 ml glomerular filtrate Tm_{PO4}/G.F.R. was calculated using the nomogram of Walton and Bijvoet (25). Serum-intact PTH and human FGF23 were measured using an ELISA (Immutopics), whereas $1,25(OH)_2D_3$ determinations were performed using a commercially available RIA kit (Immunodiagnostic Systems, Fountain Hills, AZ).

Skeletal radiography, microcomputed tomography (microCT), and bone mineral density

Femurs were removed and dissected free of soft tissue. Contact radiographs were obtained using a radiographic inspection system (model 805, Faxitron Contact, Faxitron, Germany) (22-kV voltage and 4-min exposure time). X-Omat TL film (Eastman Kodak, Rochester, NY) was used and processed routinely.

Tibiae obtained from 2-month-old mice were dissected free of soft tissue, fixed overnight in 70% ethanol, and analyzed with a microCT scanner and associated analysis software (model 1072, SkyScan, Antwerp, Belgium). Image acquisition was performed at 100 kV and 98 μA with a 0.9-degree rotation between frames. During scanning, the samples were enclosed in a tightly fitting rigid plastic rube to prevent movement. Thresholding was applied to the images to segment the bone from the background, and the same threshold setting was used for all the samples. Two-dimensional images were used to generate three-dimensional (3D) reconstructions using the 3D Creator software supplied with the instrument.

For measurement of tibial and femoral bone mineral density (BMD), a PIXImus densitometer (LUNAR Corp., Madison, WI) was used with precision of 1% coefficient of variation for skeletal BMD. The PIXImus software automatically calculated the BMD and recorded the data in Excel files (Microsoft, Redmond, CA).

Histology

Thyroparathyroidal tissue, femurs, and tibiae were removed and fixed in PLP fixative [2% paraformaldehyde containing 0.075 M lysine and 0.01 M sodium periodate) overnight at 4 C and processed histolog-

ically, as previously described (26)]. The proximal ends of the tibiae were decalcified in EDTA glycerol solution for 5–7 d at 4 C. Decalcified tibiae and other tissues were dehydrated and embedded in paraffin after which 5-μm sections were cut on a rotary microtome. The sections were stained with hematoxylin and eosin or histochemically for collagen, alkaline phosphatase (ALP), or tartrate resistant acid phosphatase (TRAP) activity as described below. Alternatively, undecalcified femora were embedded in LR White acrylic resin (London Resin Co. Ltd., London, UK), and 1-μm sections were cut on an ultramicrotome. These sections were stained for mineral either with the von Kossa staining procedure and counterstained with toluidine blue or subjected to the Goldner's-Masson-trichrome stain to discriminate mineralized from unmineralized tissues.

Histochemical staining for collagen, ALP, and TRAP

Total collagen was detected in paraffin sections using a modification of Lopez-De Leon and Rojkind (27). Dewaxed sections were exposed to 1% sirius red in saturated picric acid for 1 h. After washing with distilled water, sections were dehydrated and mounted with Biomount medium.

Enzyme histochemistry for ALP activity was performed as previously described (28, 29). Briefly, after preincubation overnight in 1% magnesium chloride in 100 mM Tris-maleate buffer (pH 9.2), dewaxed sections were incubated for 2 h at room temperature in a 100 mM Tris-maleate buffer containing naphthol AS-MX phosphate (0.2 mg/ml, Sigma) dissolved in ethylene glycol monomethyl ether (Sigma) as substrate and fast red TR (0.4 mg/ml, Sigma) as a stain for the reaction product. After washing with distilled water, the sections were counterstained with Vector methyl green nuclear counterstain (Vector Laboratories, Burlington, Ontario, Canada), and mounted with Kaiser's glycerol jelly.

Enzyme histochemistry for TRAP was performed using a modification of a previously described protocol (26). Dewaxed sections were preincubated for 20 min in buffer containing 50 mM sodium acetate and 40 mM sodium tartrate (pH 5.0). Sections were then incubated for 15 min at room temperature in the same buffer containing 2.5 mg/ml naphthol AS-MX phosphate (Sigma) in dimethylformamide as substrate and 0.5 mg/ml fast garnet GBC (Sigma) as a color indicator for the reaction product. After washing with distilled water, the sections were counterstained with methyl green and mounted in Kaiser's glycerol jelly.

Immunohistochemistry

Paraffin sections were stained immunohistochemically for aggrecan, PHEX, sodium-phosphate transport protein 2 (NPT2), and CYP27B1 using the avidin-biotin-peroxidase complex technique. Briefly, primary antibody was applied to tissues overnight at room temperature. Rabbit antiserum to bovine aggrecan (R130, courtesy of A. R. Poole, Shriners Hospital, Montréal, Canada), rabbit antiserum against a synthetic peptide, ESEEKPKEK, corresponding to residues 606–614 of the carboxyl-terminal amino acid sequence of PHEX (30), affinity-purified rabbit serum against NPT2 (courtesy of M. Knepper, Laboratory of Kidney and Electrolyte Metabolism, National Institutes of Health, Bethesda, MD), and sheep antimurine CYP27B1 IGg fraction (The Binding Site Ltd., Birmingham, UK) were employed. As negative control, preimmune serum or Tris-buffered saline was substituted for the primary antibody. After washing, tissues were incubated with secondary antibody (biotinylated rabbit antigoat IgG, biotinylated goat antirabbit IgG). Sections were then washed and incubated with the Vectastain ABC-AP reagent or the Vectastain Elite ABC reagent (Vector Laboratories) for 45 min. After washing, red pigmentation to demarcate regions of immunostaining was produced by a 10- to 15-min treatment with Fast Red TR/Naphthol AS-MX phosphate (containing 1 mM levamisole as endogenous alkaline phosphatase inhibitor; Sigma), or gray pigmentation was likewise produced using a Vector SG kit (Vector Laboratories). After washing with distilled water, the sections were counterstained with methyl green and mounted with Kaiser's glycerol jelly.

Computer-assisted image analysis

After histochemical staining of sections from six mice of each genotype, images of fields were photographed with a digital camera (Sony). Images of micrographs from single sections were digitally recorded using a rectangular template, and recordings were processed using Northern Eclipse image analysis software. For determining the trabecular bone volume relative to the total volume in collagen-stained sections, the mineralized area of hypertrophic zone, and osteoid volume relative to the BV in von Kossa-stained sections, ALP-positive area and intensity (summary total gray) in ALP histochemical-stained sections, and the number and size of osteoclasts in TRAP histochemical-stained sections, thresholds were set using green and red channels. The thresholds were determined as described previously (30, 31). The trabecular volume was measured in the metaphyseal region from below the distal (metaphyseal) side of the growth plate to 2.0 mm toward the diaphysis. ALP and TRAP parameters were measured in the fields of metaphyseal regions.

Northern blot analysis

cDNA fragments corresponding to nucleotides 535-1586 of mouse *25-hydroxyvitamin D_3 24-hydroxylase* (*Cyp24*; GenBank accession no. D49438) to nucleotides 421-1471 of mouse *25-hydroxyvitamin D_3 1-α-hydroxylase* (*Cyp27b1*; GenBank accession no. AB006034) were prepared by RT-PCR of mouse kidney RNA, subcloned, and verified by sequencing. DNA probes for *Cyp24*, *Cyp27b1*, and *glyceraldehyde-3-phosphate dehydrogenase* (*Gapdh*) were prepared by a random primed DNA labeling kit (Roche Molecular Biosciences, Indianapolis, IN) and [α-^{32}P]dCTP (800 Ci/mmol; PerkinElmer Life Sciences, Norwalk, CT). Total RNA was isolated from kidney and bone with Tripure isolation reagent (Roche Molecular Biosciences), and 20-μg aliquots were fractionated by electrophoresis on a 1% formaldehyde agarose gel, transferred to nitrocellulose membranes by upward capillary transfer in 20× saline sodium citrate (SSC) overnight, and hybridized to the radiolabeled cDNA fragment (48% formamide, 10% dextran sulfate, 5× SSC, 1× Denhardt's solution, and 100 μg/ml salmon sperm DNA) at 42 C overnight. The membranes were washed in 0.1% SDS plus 2× SSC for 15 min at room temperature and then in 0.1% SDS plus 0.1%× SSC for another 15 min at 60 C. The autoradiograms were prepared using BioMax film (Kodak) at −80 C with intensifying screens. Quantification of signal intensity on autoradiograms was performed by personal densitometer (Amersham Biosciences, Piscataway, NJ) using ImageQuant software.

Statistical analysis

Data from image analysis are presented as mean ± SEM. Statistical comparisons were made using a two-tailed unpaired *t* test, with $P < 0.05$ being considered significant.

Results

Generation of transgenic mice

Transgenic mice expressing the human mutant cDNA form *FGF23* (R176Q) under the control of the human *APOE3* promoter and its associated hepatic control region were generated (Fig. 1A). This approach was used previously to obtain mice with high levels of secreted osteoprotegerin, a protein involved in the regulation of bone density, in the systemic circulation (32, 33). Eleven mice harboring the transgene were identified by Southern blot analysis of tail DNA, and most exhibited significant growth retardation, a round back, with a short snout and tail, features that became readily apparent after weaning. Only two survived into adulthood and were able to mate and transmit the transgene (Fig. 1B). The two founders were shown to have a low- and high-copy number of the transgene inserted in the genome and expressed corresponding levels of transgene mRNA exclusively in the liver (Fig. 1C). FGF23 (R176Q) was readily detectable in liver lysates (Fig. 1D) and serum (Fig. 1E) of transgenic mice but not control mice, indicating that the transgene product was successfully expressed and delivered to the systemic circulation. For all subsequent studies, animals from both lines of transgenic mice were used.

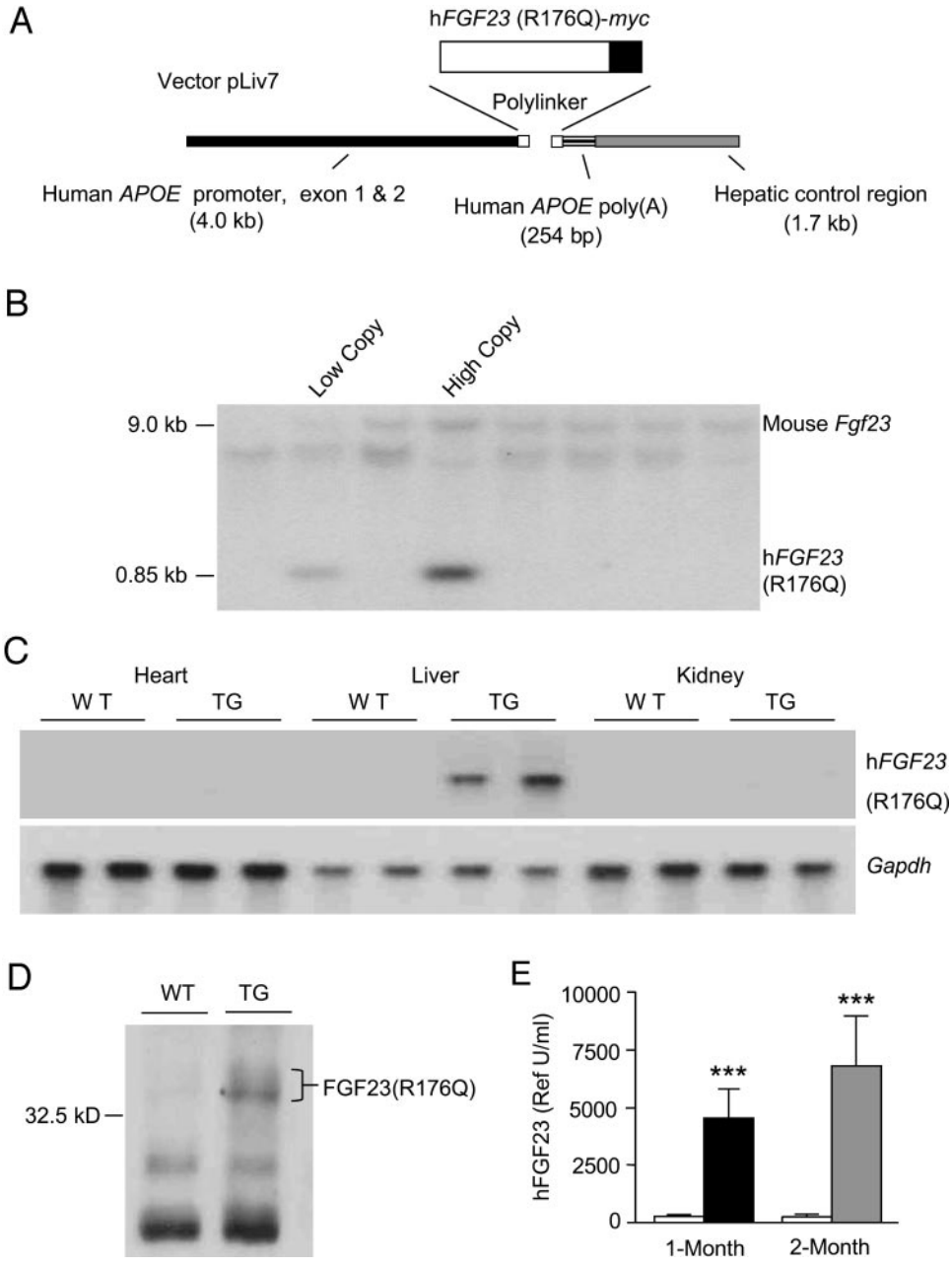

FIG. 1. Generation of FGF23 (R176Q) transgenic mice. A, Schematic representation of the human FGF23 (R176Q)-myc transgene. The *myc* epitope was inserted into the cDNA for visualization and manipulation of the recombinant protein. B, Southern blot analysis of tail genomic DNA digested with *EcoR*I and probed with radiolabeled human *FGF23* cDNA probe. Shown are DNA samples from the two surviving founders with low- and high-copy transgene number. C, Northern blot analysis for *FGF23* transcripts in tissues from wild-type (WT) and transgenic (TG) littermates. The *FGF23* (R176Q) transgene was highly expressed only in the liver of transgenic animals, whereas other tissues were devoid of it. *FGF23* transcripts were absent from all tissues examined in wild-type animals. *Gapdh* mRNA was probed as control for sample loading. D, Western blot analysis of mouse liver FGF23 (R176Q) expression using anti-myc antibody. E, Circulating FGF23 (R176Q) levels were increased in transgenic mice, with higher levels observed at 2 months of age. ***, $P < 0.001$, n = 6.

Biochemical changes due to FGF23 (R176Q) overexpression

Serum was obtained from mice at 1 and 2 months of age and analyzed (Fig. 2). High circulating levels of FGF23 (R176Q) were associated with profound hypophosphatemia with decreased renal tubular reabsorption of phosphate, increased serum ALP activity, and low serum levels of $1,25(OH)_2D_3$ that were inappropriate for the prevailing degree of hypophosphatemia. These biochemical alterations are characteristic of inherited and acquired renal phosphate-wasting states associated with elevated circulating FGF23 levels. However, in addition, unanticipated changes in parameters of calcium homeostasis were also apparent in the transgenic mice that became more pronounced with age. Serum calcium levels were slightly diminished, and this was reflected in increased circulating levels of PTH and serum ALP activity. Urinary calcium excretion was also decreased in the transgenic mice, consistent with increased renal tubular calcium reabsorption in response to circulating PTH. These findings, indicative of secondary hyperparathyroidism, were further substantiated histologically at the level of the parathyroids as the glands became progressively enlarged over time, likely a consequence of the persistent stimulus for PTH secretion arising in the setting of elevated FGF23 levels.

Skeletal effects of FGF23 (R176Q) overexpression

We next sought to investigate the skeletal abnormalities associated with FGF23 (R176Q) overexpression. In Fig. 3A are radiographs of femurs from wild-type and transgenic mice at 1 and 2 months of age. The transgenic bones were

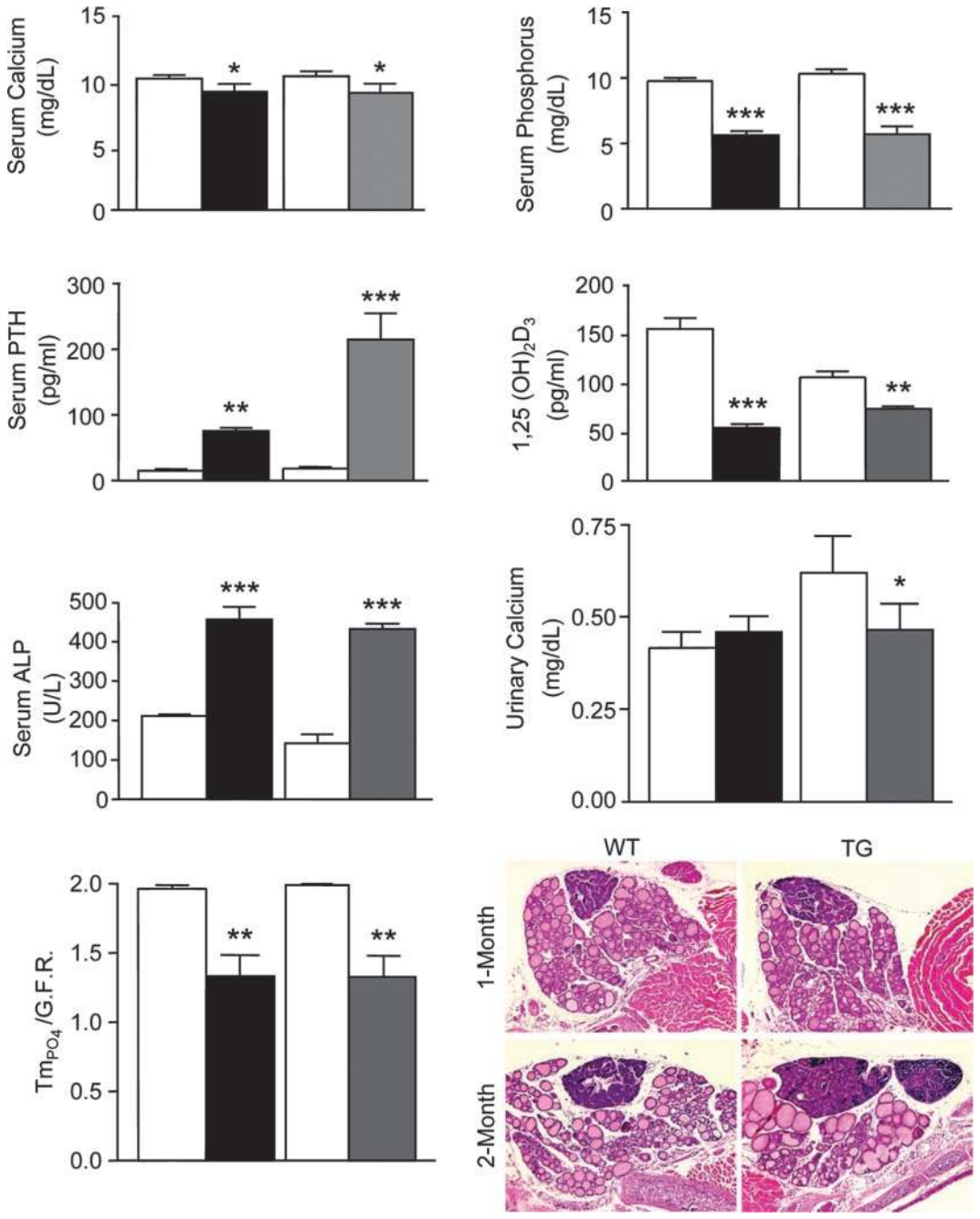

FIG. 2. Serum biochemistry and parathyroid gland histology. A, Serum levels for inorganic phosphate, $1,25(OH)_2D_3$, calcium, PTH, and ALP activity and urinary calcium and renal tubular phosphate reabsorption. *Open bars* indicate wild-type animals at 1 (*left*) and 2 (*right*) months of age. The *solid bars* represent transgenic mice at 1 month and *gray bars* at 2 months of age. *, $P < 0.05$, **, $P < 0.01$, ***, $P < 0.001$, n = 8. B, Parathyroid gland histology at 1 and 2 months of age, showing progressive gland hyperplasia in the transgenic animals (magnification, ×100).WT, Wild-type; TG, transgene.

proportionately smaller in size and more radiolucent than their wild-type counterparts. The frontal view of 3D reconstructed proximal end of tibia obtained using microCT showed the wider, unmineralized growth plate in the transgenic mice (Fig. 3B). The reduced skeletal mineralization was subsequently confirmed on histological sections of the epiphyseal region of femurs as shown in Fig. 3C. In comparison with wild-type animals, growth plates from transgenic mice expressing FGF23 (R176Q) were wider, more disorganized, and less well mineralized (Fig. 3, D and E), consistent with an advanced form of rickets. These rachitic changes were more apparent in transgenic animals at 2 months of age.

Although trabecular volume was increased in FGF23 (R176Q) transgenic mice, compared with wild-type (Fig. 4A), mineralized trabeculae were much less numerous as demonstrated by 3D reconstructed longitudinal sections of long bones obtained from microCT scans (Fig. 4B) and histological assessment (Fig. 3C). Profound osteomalacic

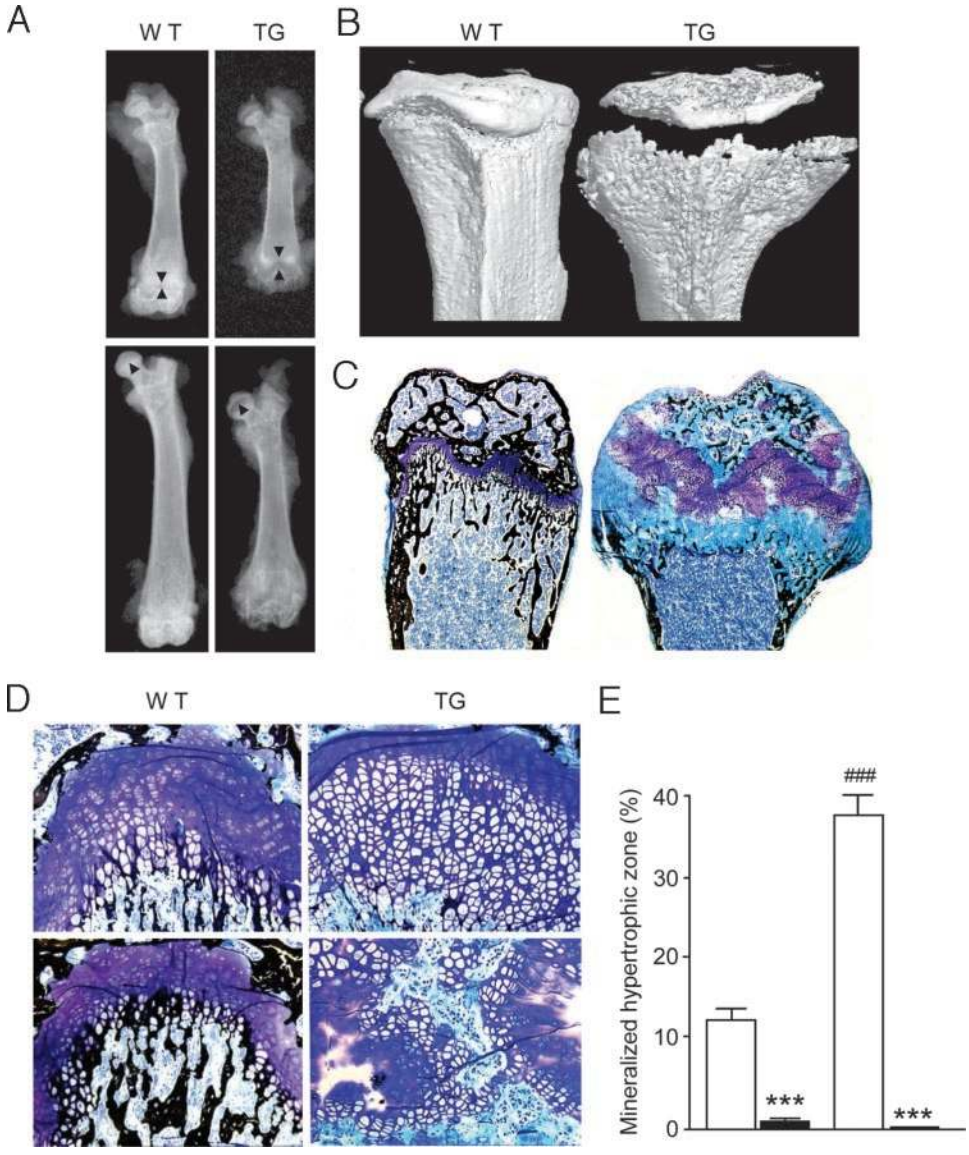

FIG. 3. Radiographic, microCT, and histological growth plate alterations. A, Radiographs of femurs from wild-type (WT) and transgenic (TG) mice at 1 (*top panels*) and 2 (*lower panels*) months of age. *Arrowheads* outline the widened, undermineralized growth plates in the transgenic specimens. B, Three-dimensional reconstruction of microCT scans of the proximal tibial metaphysis from 2-month-old WT and TG mice illustrating the widening of the growth plate and poor mineralization of the TG bones. C and D, Low (×5) and high (×200) magnification of Von Kossa staining of distal ends of femurs, demonstrating histologically the widening of the growth plate and impaired mineralization of the hypertrophic zone in transgenic animals. D, Quantitative assessment of the mineralized portion of the hypertrophic zone of the growth plate. ***, $P < 0.001$ between WT and TG mice; ###, $P < 0.001$ between TG mice at 1 and 2 months of age, n = 6.

changes were apparent in trabecular and cortical bone because increased amounts of unmineralized osteoid was present in specimens from animals expressing FGF23 (R176Q) (Fig. 4, C and D). In addition to the impairment in bone matrix mineralization, bone resorption was also diminished in the transgenic mice as indicated by the low osteoclast number (Fig. 4E) and the persistence of aggrecan expression and chondrocytes in the bone trabeculae (Fig. 4F). In contrast, ALP activity was increased in the transgenic bones (Fig. 4G). Interestingly, PHEX expression was enhanced in this pathophysiological state because intense protein immunoreactivity was observed in growth plate chondrocytes (not shown), osteoblasts, and osteocyte cell bodies and canalicular cellular processes, specifically in regions of unmineralized bone (Fig. 4H). BMD measurements and histomorphometric analysis further confirmed and quantified the reduced BMD and other skeletal alterations arising from FGF23 (R176Q) overexpression (Fig. 5, A–F).

Renal Effects of FGF23 (R176Q)

Given the profound phosphaturia associated with FGF23 (R176Q) overexpression, we next sought to examine the expression of renal Npt2 in the renal proximal tubule epithelial cells of transgenic mice at 2 months of age. Immunoreactivity for the protein was markedly diminished in the presence of high circulating levels of FGF23 (R176Q) and the concurrent rise in serum PTH concentration (Fig. 6A). These changes are likely to account, therefore, for the impairment in tubular phosphate reabsorption and inappropriate excretion of urinary phosphate in these animals.

Despite the marked hypophosphatemia, expected alterations in the expression of renal hydroxylases aimed at increasing circulating levels of $1,25(OH)_2D_3$ failed to take place. Rather, instead of the anticipated decrease, transcript levels for *Cyp24* in transgenic kidneys were in fact progressively increased at 1 and 2 months of age, com-

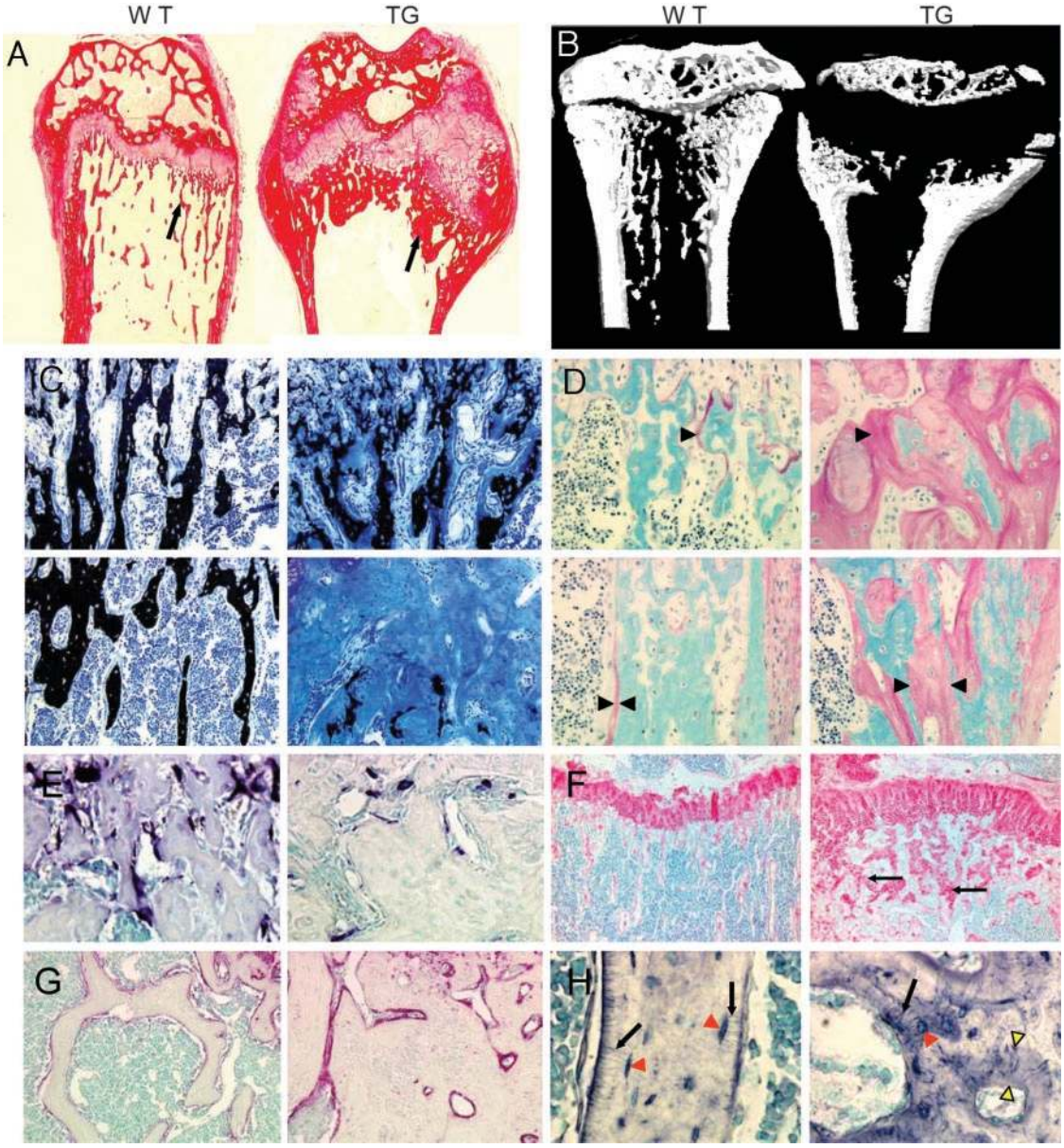

FIG. 4. Bone alterations and PHEX expression. A, Total collagen staining using sirius red at 2 months of age (magnification, ×25). *Arrows* indicate trabecular bone. WT, Wild-type; TG, transgene. B, MicroCT scan-derived longitudinal sections of the proximal tibial metaphysis from 2-month-old WT and TG mice showing the widening metaphysis and growth plate and poor mineralization of the trabecules. C, Von Kossa staining of trabecular bone illustrating the increased BV and osteoid content in the transgenic specimens. *Top panels*, 1 month; *bottom panels*, 2 months (magnification, ×200). D, Longitudinal undecalcified long bone sections from 2-month-old mice subjected to the Goldner's-Masson-trichrome stain to discriminate mineralized (*blue/green*) from unmineralized (*pink/red*) bone tissue. Increased osteoid (*arrowheads*) was noted in both trabecular (*top panels*) and cortical (*bottom panels*) bone of transgenic mice (magnification, ×200). E, Histochemical staining for TRAP activity at 2 months of age (magnification, ×400). F, Aggregan expression by immunohistochemistry at 2 months of age. Note persistence of chondrocytes in trabecular bone (*arrows*) (magnification, ×200). G, Histochemical staining for ALP activity at 2 months of age (magnification, ×400). H, Phex immunoreactivity in osteoblasts/osteocytes. Prominent PHEX expression is present in cell bodies (*red arrowheads*), canalicular processes of osteocytes (*arrows*), and unmineralized regions of newly laid-down bone (region between the two *yellow arrowheads*) (magnification, ×400).

pared with controls (Fig. 6, B and C). On the other hand, mRNA levels for renal *Cyp27b1* were increased (Fig. 7, A and B), but this failed to translate to increased protein immunoreactivity at the level of the renal proximal tubule (Fig. 7C), suggesting that a decrease in Cyp27b1 activity likely results from a defect in translational or posttranslational modification of the enzyme.

Discussion

Here we show that transgenic mice overexpressing FGF23 (R176Q) recapitulate the biochemical [hypophosphatemia, decreased renal tubular phosphate reabsorption, low circulating levels of $1,25(OH)_2D_3$] and skeletal abnormalities (rickets and osteomalacia) reported in patients with hypophosphatemic

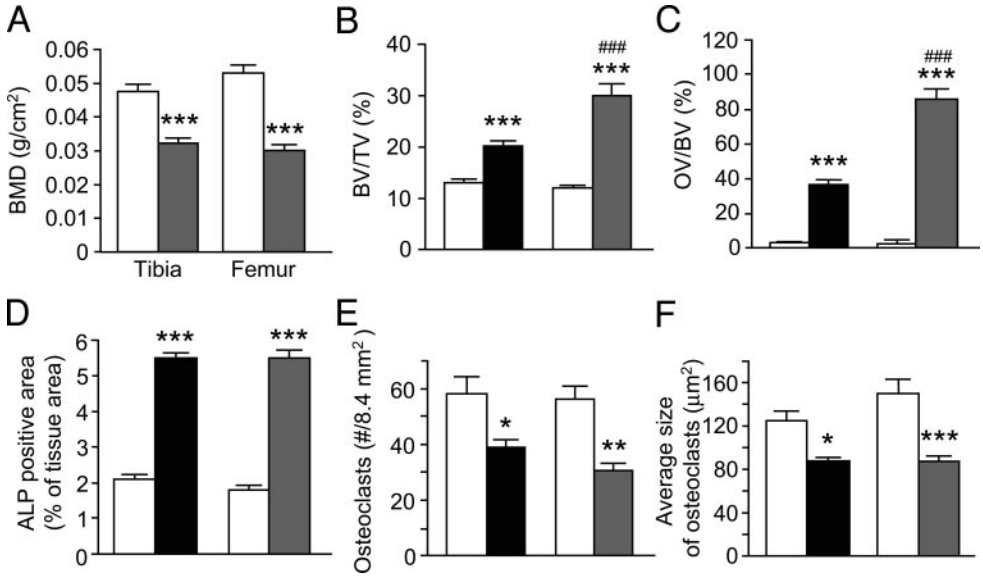

FIG. 5. BMD and quantitative histomorphometry. A, BMD measurements using dual-energy x-ray absorptiometry at the proximal end of tibia and distal femoral metaphysis at 2 months of age. B, BV/total volume, BV over total volume. C, OV/BV, osteoid volume over BV. D, ALP-positive stained area. E, Osteoclast number. F, Average osteoclast size. *, $P < 0.05$, **, $P < 0.01$, ***, $P < 0.001$ between wild-type and transgenic mice; ###, $P < 0.001$ between transgenic mice at 1 and 2 months of age, n = 6.

states associated with high circulating levels of FGF23 such as XLH, ADHR, TIO, and fibrous dysplasia. The phenotypic similarities between these renal phosphate-wasting disorders suggest that alterations by the same phosphate-regulating factor, likely FGF23, underlie their pathogenesis.

Whereas similar observations were recently published by others, significant differences are apparent between the two studies. Shimada *et al.* (34) reported that serum calcium and PTH levels in the transgenic mice were lower than those of normal mice. In contrast, we consistently observed a mild decrease in serum calcium accompanied by a corresponding rise in circulating PTH levels in transgenic animals, similar to what we previously reported after implantation of nude mice with tumors that oversecrete FGF23 into the circulation (17). These findings (high circulating PTH but low-normal serum calcium) were in part confirmed in a third study published while this work was under review (35). Presently it remains unclear as to the reason for the observed discrepancy in parameters of calcium homeostasis between the various transgenic animal models. It is possible these differences may arise from different promoter usage [*ApoE3 vs.* chicken *β-actin vs.* α1(I) *collagen*], although this is unlikely. The phenotypic similarities in mice expressing FGF23 in hepatocytes (*ApoE3*) or osteoblasts [α1(I) *collagen*] would indicate that the biological effects of FGF23 are likely endocrine rather than acting locally on bone cells. Alternatively, the form of the protein overexpressed by the transgene is more likely to impact on the findings because the FGF23 (R176Q) protein would exert derangements more profound than the wild-type form, perhaps due to its prolonged biological half-life (17).

Abnormalities in parameters of calcium homeostasis are not consistently observed in patients with renal phosphate-wasting disorders. Although serum calcium levels are usually normal, mild hypocalcemia has been described in patients with XLH and TIO (18). Moreover, a trend toward higher PTH levels has been reported in patients with ADHR (2), whereas apparent secondary and even tertiary hyperparathyroidism has been reported in XLH patients not treated with phosphate and $1,25(OH)_2D_3$ (21, 36–39). Secondary hyperparathyroidism with increased circulating levels of PTH has also been reported in *Hyp* and *Gy* mice, the murine homologs of XLH (40, 41). Serum levels of PTH have been variably reported as low as well as elevated but are most frequently normal in TIO (21, 42, 43). The reason for the discrepancy between these clinical observations and our findings can be explained, in part, by the fact that in our animal model, deregulated overexpression would tend to raise more profoundly the circulating levels of FGF23. Conceivably, in patients with renal phosphate-wasting disorders, potential feedback mechanisms are set in motion to restrain its excess production. In a recent study, FGF23 concentrations were 481 ± 528 RefU/ml in patients with suspected oncogenic osteomalacia and 353 ± 510 RefU/ml in XLH patients, approximately 6% of the serum FGF23 levels determined in our transgenic mice. Whereas the nature of such mechanisms remains unclear, the apparent reversal of the phenotype in a number of patients with ADHR (2) corroborates their existence.

Although the pathophysiology of hyperparathyroidism in hypophosphatemic rickets remains unclear at present (44), abnormal PTH regulation has been suggested (37). Given the high abundance of *PHEX* mRNA in parathyroid glands of patients with XLH (39), PHEX may play a role in the regulation of PTH, perhaps by altering its cleavage within or outside the parathyroid gland either directly (45) or indirectly (46, 47). Alternatively, elevated PTH levels could be readily attributed to the decreased levels of $1,25(OH)_2D_3$ synthesis, thereby leading to hypocalcemia. PTH secretion appropriately ensues aimed toward maintaining calcium homeostasis by increasing bone turnover (increased serum ALP activity) and decreasing urinary calcium excretion, all consistent with secondary hyperparathyroidism. Additional confirmatory support for this argument is provided by the diffuse parathyroid hyperplasia observed histologically in transgenic animals that became progressively pronounced with age. Interestingly, it was suggested recently that elevated levels of circulating FGF23 also promote the develop-

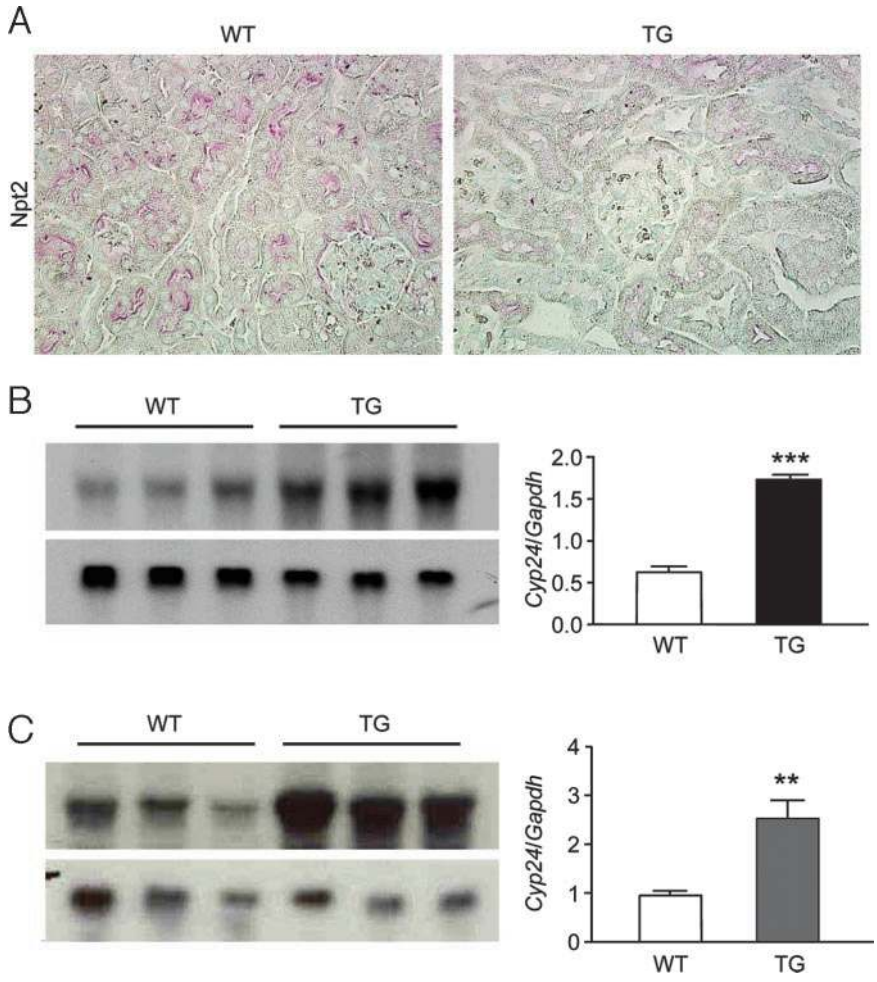

FIG. 6. Npt2 and *Cyp24* expression. A, Npt2 immunoreactivity in proximal renal tubule cells from wild-type (WT) and transgenic (TG) mice at 2 months of age (magnification, ×200). Northern blot analysis of *Cyp24* mRNA expression at 1 (B) and 2 (C) months of age. *Gapdh* mRNA was probed as control to correct for variations in sample loading. Graphs illustrate the ratio of *Cyp24* to *Gapdh* expression at each of the indicated time periods. Shown are representative samples from three mice from each group. *, $P < 0.05$, ***, $P < 0.001$, n = 12.

ment of secondary hyperparathyroidism in predialysis patients through suppression of CYP27B1 activity (48).

What then is the cause for the decrease in circulating levels of $1,25(OH)_2D_3$? It is rather remarkable that when FGF23 is overexpressed, a rise in circulating PTH levels ensues, which fails to normalize $1,25(OH)_2D_3$ serum concentrations. Normally the renal hydroxylases Cyp27b1 and Cyp24 are very tightly and reciprocally regulated by PTH, which induces Cyp27b1 while down-regulating Cyp24 activity by making the *Cyp24* mRNA susceptible to degradation (49, 50). Here we show that at 1 month of age, in mice overexpressing FGF23, Cyp27b1 expression, at least at the mRNA level, is decreased, whereas concurrently, *Cyp24* transcript levels are increased, compared with littermates devoid of the transgene. These are effects that are diametrically opposed to what one would anticipate in the presence of high circulating PTH levels and the concomitant hypophosphatemia. Yet, as these animals age and PTH levels become more pronounced, this is paralleled by a corresponding increase in both renal *Cyp24* and *Cyp27b1* mRNA expression, compared with controls. Yet these alterations were again not reflected in corresponding rises in $1,25(OH)_2D_3$ circulating levels. Two possibilities could account for this discrepancy: first, the relentless metabolism of $1,25(OH)_2D_3$ to inactive forms by the rising levels of *Cyp24*, and second, by the observation that the rise in *Cyp27b1* mRNA levels is not reflected by similar alterations at the protein levels. In fact, in our mice renal tubular Cyp27b1 immunoreactivity is comparable with that in wild-type specimens. This dichotomy between transcript and protein levels for Cyp27b1 and the inability of PTH and hypophosphatemia to stimulate its enzymatic activity have also been described recently in *Hyp* mice (51). Therefore, the defect in Cyp27b1 activity does not result from aberrant transcriptional regulation but likely from a defect in translational or posttranslational modification.

Our findings here support the scheme that increased circulating levels of FGF23 not only decrease Npt2 expression and renal tubular phosphate reabsorption but also, either directly or indirectly, impair regulation of *Cyp24* expression by PTH and alter *Cyp27b1* mRNA translation or posttranslational modification of the protein. FGF23, therefore, appears to be directly or indirectly responsible for the inappropriate alterations in the activity of the renal vitamin D-metabolizing hydroxylases observed both in our mice and likely in patients with ADHR, TIO, and XLH. This may also explain, in part, the inappropriately low-normal levels of $1,25(OH)_2D_3$ associated with these three disorders despite the prevailing hypophosphatemia, a finding that is rather unique to them because in other renal phosphate-wasting states, synthesis of $1,25(OH)_2D_3$ is up-regulated. For example, $1,25(OH)_2D_3$ synthesis is appropriately increased by

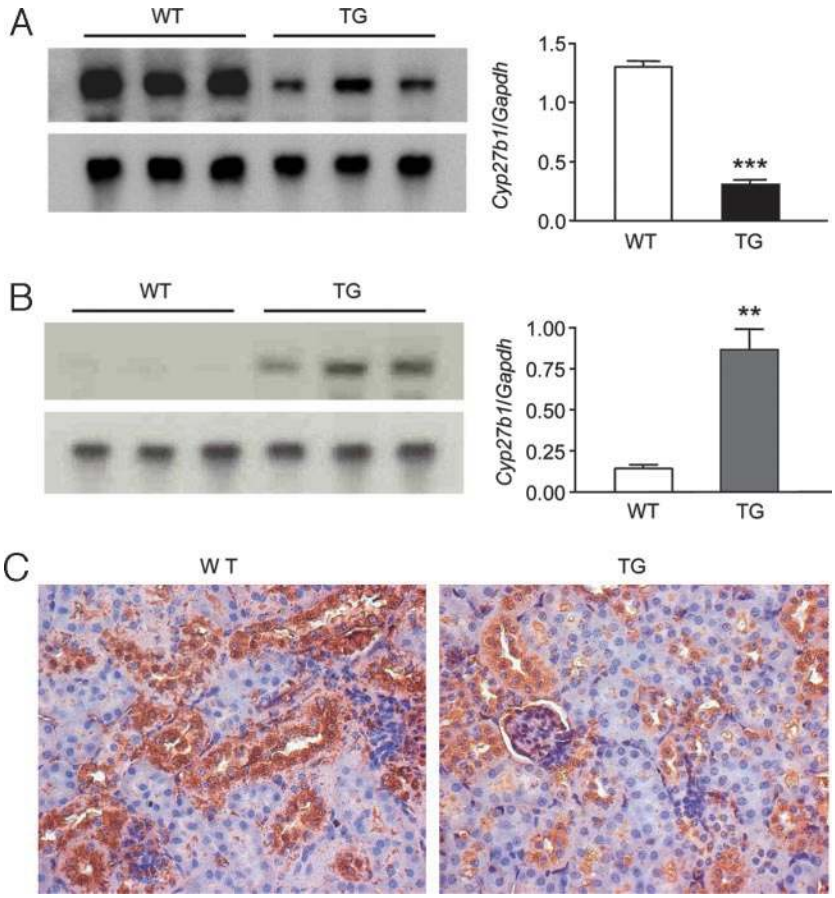

FIG. 7. Renal Cyp27b1 expression. Northern blot analysis of renal *Cyp27b1* mRNA expression at 1 (A) and 2 (B) months of age. *Gapdh* mRNA was probed as control to correct for variations in sample loading. Graphs illustrate the ratio of *Cyp27b1* to *Gapdh* expression at the indicated time periods. Shown are representative samples from three mice from each group. *, $P < 0.05$, ***, $P < 0.001$, n = 12. C, Cyp27b1 immunoreactivity in proximal renal tubule cells from wild-type (WT) and transgenic (TG) mice at 2 months of age (magnification, ×400).

hypophosphatemia in *Npt2*-null mice (52) and patients with hypophosphatemia associated with heterozygote missense mutations in the *NPT2* gene (53). Further studies will be necessary to define the mechanisms that underlie these defects.

The question then arises as to whether the increase in circulating PTH contributes, at least in part, to the decrease in Npt2 action at the level of the renal proximal tubule and the inappropriate phosphaturia associated with this condition. Shimada *et al.* (34) concluded that the reduction in Npt2 expression and hypophosphatemia in their transgenic mice appear to be induced by a PTH-independent mechanism. In contrast, based on our animal model, it is becoming apparent that in the presence of high serum FGF23 levels, a dissociation of PTH actions at the level of the kidney occurs, whereby the effects of PTH on reabsorbing urinary calcium and perhaps promoting phosphaturia by reducing Npt2 expression are preserved, whereas Cyp27b1 activity and *Cyp24* expression are refractory to its action. The concept that hyperparathyroidism can contribute to the phosphate loss independent of that arising from the *PHEX* mutation is also supported by the observation that parathyroidectomy in patients with XLH can lead to an increase in serum phosphate (39). Experiments are presently underway using mice carrying targeted disruption of the *Pth* gene (54) to investigate this possibility.

In summary, we have generated a murine model of FGF23 overexpression that has provided us with new insights into the complex cascade of factors that underlie the pathophysiology of renal phosphate-wasting disorders. This animal model will now serve to further clarify the role of PTH in the phosphaturic process and define the molecular mechanisms by which FGF23 alters renal vitamin D metabolism in these conditions.

Acknowledgments

Received February 23, 2004. Accepted July 22, 2004.

Address all correspondence and requests for reprints to: Andrew C. Karaplis, Division of Endocrinology, Department of Medicine, Sir Mortimer B. Davis-Jewish General Hospital, 3755 Cote Ste. Catherine Road, Montréal, Québec, Canada H3T 1E2. E-mail: akarapli@ldi.jgh.mcgill.ca.

This work was supported by grants from the Canadian Institutes of Health (CIHR), the National Cancer Institute of Canada, and the Canadian Arthritis Network. A.C.K. is recipient of a CIHR Scientist Award.

References

1. **Carpenter TO** 1997 New perspectives on the biology and treatment of X-linked hypophosphatemic rickets. Pediatr Clin North Am 44:443–466
2. **Econs MJ, McEnery PT** 1997 Autosomal dominant hypophosphatemic rickets/osteomalacia: clinical characterization of a novel renal phosphate-wasting disorder. J Clin Endocrinol Metab 82:674–681
3. **Kumar R** 2000 Tumor-induced osteomalacia and the regulation of phosphate homeostasis. Bone 27:333–338
4. **Dent CE, Gertner JM** 1976 Hypophosphataemic osteomalacia in fibrous dysplasia. Q J Med 45:411–420
5. **Shimada T, Mizutani S, Muto T, Yoneya T, Hino R, Takeda S, Takeuchi Y, Fujita T, Fukumoto S, Yamashita T** 2001 Cloning and characterization of FGF23 as a causative factor of tumor-induced osteomalacia. Proc Natl Acad Sci USA 98:6500–6505
6. **Strewler GJ** 2001 FGF23, hypophosphatemia, and rickets: has phosphatonin been found? Proc Natl Acad Sci USA 98:5945–5946
7. **Silve C, Beck L** 2002 Is FGF23 the long sought after phosphaturic factor phosphatonin? Nephrol Dial Transplant 17:958–961

8. **Tenenhouse HS, Sabbagh Y** 2002 Novel phosphate-regulating genes in the pathogenesis of renal phosphate wasting disorders. Pflugers Arch 444:317–326
9. **Quarles LD** 2003 FGF23, PHEX, and MEPE regulation of phosphate homeostasis and skeletal mineralization. Am J Physiol Endocrinol Metab 285:E1–E9
10. **Berndt T, Craig TA, Bowe AE, Vassiliadis J, Reczek D, Finnegan R, Jan De Beur SM, Schiavi SC, Kumar R** 2003 Secreted frizzled-related protein 4 is a potent tumor-derived phosphaturic agent. J Clin Invest 112:785–794
11. **Shimada T, Kakitani M, Yamazaki Y, Hasegawa H, Takeuchi Y, Fujita T, Fukumoto S, Tomizuka K, Yamashita T** 2004 Targeted ablation of Fgf23 demonstrates an essential physiological role of FGF23 in phosphate and vitamin D metabolism. J Clin Invest 113:561–568
12. **The HYP Consortium** 1995 A gene (PEX) with homologies to endopeptidases is mutated in patients with X-linked hypophosphatemic rickets. Nat Genet 11:130–136
13. **The ADHR Consortium** 2000 Autosomal dominant hypophosphataemic rickets is associated with mutations in FGF23. Nat Genet 26:345–348
14. **White KE, Carn G, Lorenz-Depiereux B, Benet-Pages A, Strom TM, Econs MJ** 2001 Autosomal-dominant hypophosphatemic rickets (ADHR) mutations stabilize FGF-23. Kidney Int 60:2079–2086
15. **Seufert J, Ebert K, Muller J, Eulert J, Hendrich C, Werner E, Schuuze N, Schulz G** 2001 Octreotide therapy for tumor-induced osteomalacia. N Engl J Med 345:1883–1888
16. **Riminucci M, Collins MT, Fedarko NS, Cherman N, Corsi A, White KE, Waguespack S, Gupta A, Hannon T, Econs MJ, Bianco P, Gehron Robey P** 2003 FGF-23 in fibrous dysplasia of bone and its relationship to renal phosphate wasting. J Clin Invest 112:683–692
17. **Bai XY, Miao D, Goltzman D, Karaplis AC** 2003 The autosomal dominant hypophosphatemic rickets R176Q mutation in fibroblast growth factor 23 resists proteolytic cleavage and enhances *in vivo* biological potency. J Biol Chem 278:9843–9849
18. **Carpenter TO** 2003 Oncogenic osteomalacia: a complex dance of factors. N Engl J Med 348:1705–1708
19. **Yamazaki Y, Okazaki R, Shibata M, Hasegawa Y, Satoh K, Tajima T, Takeuchi Y, Fujita T, Nakahara K, Yamashita T, Fukumoto S** 2002 Increased circulatory level of biologically active full-length FGF-23 in patients with hypophosphatemic rickets/osteomalacia. J Clin Endocrinol Metab 87:4957–4960
20. **Weber TJ, Liu S, Indridason OS, Quarles LD** 2003 Serum FGF23 levels in normal and disordered phosphorus homeostasis J Bone Miner Res 18:1227–1234
21. **Jonsson KB, Zahradnik R, Larsson T, White KE, Sugimoto T, Imanishi Y, Yamamoto T, Hampson G, Koshiyama H, Ljunggren O, Oba K, Yang IM, Miyauchi A, Econs MJ, Lavigne J, Juppner H** 2003 Fibroblast growth factor 23 in oncogenic osteomalacia and X-linked hypophosphatemia. N Engl J Med 348:1656–1663
22. **Bowe AE, Finnegan R, Jan de Beur SM, Cho J, Levine MA, Kumar R, Schiavi SC** 2001 FGF-23 inhibits renal tubular phosphate transport and is a PHEX substrate. Biochem Biophys Res Commun 284:977–981
23. **Campos M, Couture C, Hirata IY, Juliano MA, Loisel TP, Crine P, Juliano L, Boileau G, Carmona AK** 2003 Human recombinant endopeptidase PHEX has a strict S1′ specificity for acidic residues and cleaves peptides derived from fibroblast growth factor-23 and matrix extracellular phosphoglycoprotein. Biochem J 373:271–279
24. **Liu S, Guo R, Simpson LG, Xiao ZS, Burnham CE, Quarles LD** 2003 Regulation of fibroblastic growth factor 23 expression but not degradation by PHEX. J Biol Chem 278:37419–37426
25. **Walton RJ, Bijvoet OL** 1975 Nomogram for derivation of renal threshold phosphate concentration. Lancet 2:309–310
26. **Miao D, Scutt A** 2002 Recruitment, augmentation and apoptosis of rat osteoclasts in 1,25-(OH)2D3 response to short-term treatment with 1,25-dihydroxyvitamin D3 *in vivo*. BMC Musculoskelet Disord 3:16
27. **Lopez-De Leon A, Rojkind M** 1985 A simple micromethod for collagen and total protein determination in formalin-fixed paraffin-embedded sections. J Histochem Cytochem 33:737–743
28. **He B, Deckelbaum RA, Miao D, Lipman ML, Pollak M, Goltzman D, Karaplis AC** 2001 Tissue-specific targeting of the Pthrp gene: the generation of mice with floxed alleles. Endocrinology 142:2070–2077
29. **Miao D, Scutt A** 2002 Histochemical localization of alkaline phosphatase activity in decalcified bone and cartilage. J Histochem Cytochem 50:333–340
30. **Miao D, Bai X, Panda D, McKee M, Karaplis A, Goltzman D** 2001 Osteomalacia in hyp mice is associated with abnormal phex expression and with altered bone matrix protein expression and deposition. Endocrinology 142:926–939
31. **Bai X, Miao D, Panda D, Grady S, McKee MD, Goltzman D, Karaplis AC** 2002 Partial rescue of the Hyp phenotype by osteoblast-targeted PHEX (phosphate-regulating gene with homologies to endopeptidases on the X chromosome) expression. Mol Endocrinol 16:2913–2925
32. **Simonet WS, Bucay N, Lauer SJ, Taylor JM** 1993 A far-downstream hepatocyte-specific control region directs expression of the linked human apolipoprotein E and C-I genes in transgenic mice. J Biol Chem 268:8221–8229
33. **Simonet WS, Lacey DL, Dunstan CR, Kelley M, Chang MS, Luthy R, Nguyen HQ, Wooden S, Bennett L, Boone T, Shimamoto G, DeRose M, Elliott R, Colombero A, Tan HL, Trail G, Sullivan J, Davy E, Bucay N, Renshaw-Gegg L, Hughes TM, Hill D, Pattison W, Campbell P, Sander S, Van G, Tarpley J, Derby P, Lee R, Boyle WJ** 1997 Osteoprotegerin: a novel secreted protein involved in the regulation of bone density. Cell 89:309–319
34. **Shimada T, Urakawa I, Yamazaki Y, Hasegawa H, Hino R, Yoneya T, Takeuchi Y, Fujita T, Fukumoto S, Yamashita T** 2004 FGF-23 transgenic mice demonstrate hypophosphatemic rickets with reduced expression of sodium phosphate cotransporter type IIa. Biochem Biophys Res Commun 314:409–414
35. **Larsson T, Marsell R, Schipani E, Ohlsson C, Ljunggren O, Tenenhouse HS, Juppner H, Jonsson KB** 2004 Transgenic mice expressing Fibroblast growth factor 23 under the control of the α1(I) collagen promoter exhibit growth retardation, osteomalacia, and disturbed phosphate homeostasis. Endocrinology 145:3087–3094
36. **Sullivan W, Carpenter T, Glorieux F, Travers R, Insogna K** 1992 A prospective trial of phosphate and 1,25-dihydroxyvitamin D3 therapy in symptomatic adults with X-linked hypophosphatemic rickets. J Clin Endocrinol Metab 75:879–885
37. **Carpenter TO, Mitnick MA, Ellison A, Smith C, Insogna KL** 1994 Nocturnal hyperparathyroidism: a frequent feature of X-linked hypophosphatemia. J Clin Endocrinol Metab 78:1378–1383
38. **Knudtzon J, Halse J, Monn E, Nesland A, Nordal KP, Paus P, Seip M, Sund S, Sodal G** 1995 Autonomous hyperparathyroidism in X-linked hypophosphataemia. Clin Endocrinol (Oxf) 42:199–203
39. **Blydt-Hansen TD, Tenenhouse HS, Goodyer P** 1999 PHEX expression in parathyroid gland and parathyroid hormone dysregulation in X-linked hypophosphatemia. Pediatr Nephrol 13:607–611
40. **Kiebzak GM, Roos BA, Meyer Jr RA** 1982 Secondary hyperparathyroidism in X-linked hypophosphatemic mice. Endocrinology 111:650–652
41. **Meyer Jr RA, Meyer MH, Morgan PL** 1996 Effects of altered diet on serum levels of 1,25-dihydroxyvitamin D and parathyroid hormone in X-linked hypophosphatemic (Hyp and Gy) mice. Bone 18:23–28
42. **Ryan WG, Gitelis S, Charters JR** 1986 Studies in a patient with tumor-induced hypophosphatemic osteomalacia. Calcif Tissue Int 38:358–362
43. **Yang IM, Park YK, Hyun YJ, Kim DY, Woo JT, Kim SW, Kim JW, Kim YS, Choi YK** 1997 Oncogenic osteomalacia caused by a phosphaturic mesenchymal tumor of the oral cavity: a case report. Korean J Intern Med 12:89–95
44. **Schmitt CP, Mehls O** 2004 The enigma of hyperparathyroidism in hypophosphatemic rickets. Pediatr Nephrol 19:473–477
45. **Lipman ML, Panda D, Bennett HP, Henderson JE, Shane E, Shen Y, Goltzman D, Karaplis AC** 1998 Cloning of human PEX cDNA. Expression, subcellular localization, and endopeptidase activity. J Biol Chem 273:13729–13737
46. **Boileau G, Tenenhouse HS, Desgroseillers L, Crine P** 2001 Characterization of PHEX endopeptidase catalytic activity: identification of parathyroid-hormone-related peptide107–139 as a substrate and osteocalcin, PPi and phosphate as inhibitors. Biochem J 355(Pt 3):707–713
47. **Guo R, Liu S, Spurney RF, Quarles LD** 2001 Analysis of recombinant Phex: an endopeptidase in search of a substrate. Am J Physiol Endocrinol Metab 281:E837–E847
48. **Shigematsu T, Kazama JJ, Yamashita T, Fukumoto S, Hosoya T, Gejyo F, Fukagawa M** 2004 Possible involvement of circulating fibroblast growth factor 23 in the development of secondary hyperparathyroidism associated with renal insufficiency. Am J Kidney Dis 44:250–256
49. **Zierold C, Reinholz GG, Mings JA, Prahl JM, DeLuca HF** 2000 Regulation of the porcine 1,25-dihydroxyvitamin D3–24-hydroxylase (CYP24) by 1,25-dihydroxyvitamin D3 and parathyroid hormone in AOK-B50 cells. Arch Biochem Biophys 381:323–327
50. **Zierold C, Mings JA, DeLuca HF** 2001 Parathyroid hormone regulates 25-hydroxyvitamin D(3)-24-hydroxylase mRNA by altering its stability. Proc Natl Acad Sci USA 98:13572–13576
51. **Fujiwara I, Aravindan R, Horst RL, Drezner MK** 2003 Abnormal regulation of renal 25-hydroxyvitamin D-1α-hydroxylase activity in X-linked hypophosphatemia: a translational or posttranslational defect. J Bone Miner Res 18:434–442
52. **Beck L, Karaplis AC, Amizuka N, Hewson AS, Ozawa H, Tenenhouse HS** 1998 Targeted inactivation of Npt2 in mice leads to severe renal phosphate wasting, hypercalciuria, and skeletal abnormalities. Proc Natl Acad Sci USA 95:5372–5377
53. **Prie D, Huart V, Bakouh N, Planelles G, Dellis O, Gerard B, Hulin P, Benque-Blanchet F, Silve C, Grandchamp B, Friedlander G** 2002 Nephrolithiasis and osteoporosis associated with hypophosphatemia caused by mutations in the type 2a sodium-phosphate cotransporter. N Engl J Med 347:983–991
54. **Miao D, He B, Lanske B, Bai XY, Tong XK, Hendy GN, Goltzman D, Karaplis AC** 2004 Skeletal abnormalities in Pth-null mice are influenced by dietary calcium. Endocrinology 145:2046–2053

***Endocrinology* is published monthly by The Endocrine Society (http://www.endo-society.org), the foremost professional society serving the endocrine community.**